

# VASparse: Towards Efficient Visual Hallucination Mitigation for Large Vision-Language Model via Visual-Aware Sparsification

Xianwei Zhuang, Zhihong Zhu, Yuxin Xie, Liming Liang, Yuexian Zou \*  
 SECE of Peking University  
 xwzhuang@stu.pku.edu.cn

## Abstract

Large Vision-Language Models (LVLMs) may produce outputs that are unfaithful to reality, also known as visual hallucinations (VH), which significantly impedes their real-world usage. To alleviate VH, various decoding strategies have been proposed to enhance visual information. However, many of these methods may require secondary decoding and rollback, which significantly reduces inference speed. In this work, we propose an efficient plug-and-play decoding algorithm via Visual-Aware Sparsification (VASparse) from the perspective of token sparsity for mitigating VH. VASparse is inspired by empirical observations: (1) the sparse activation of attention in LVLMs, and (2) visual-agnostic tokens sparsification exacerbates VH. Based on these insights, we propose a novel token sparsification strategy that balances efficiency and trustworthiness. Specifically, VASparse implements a visual-aware token selection strategy during decoding to reduce redundant tokens while preserving visual context effectively. Additionally, we innovatively introduce a sparse-based visual contrastive decoding method to recalibrate the distribution of hallucinated outputs without the time overhead associated with secondary decoding. Subsequently, VASparse recalibrates attention scores to penalize attention sinking of LVLMs towards text tokens. Extensive experiments across four popular benchmarks confirm the effectiveness of VASparse in mitigating VH across different LVLM families without requiring additional training or post-processing. Impressively, VASparse achieves state-of-the-art performance for mitigating VH while maintaining competitive decoding speed. Code is available at <https://github.com/mengchuang123/VASparse-github>.

## 1. Introduction

Motivated by the success of Large Language Models (LLMs), large vision-language models (LVLMs) have made significant advancements in cross-modal understanding and

\*Corresponding author

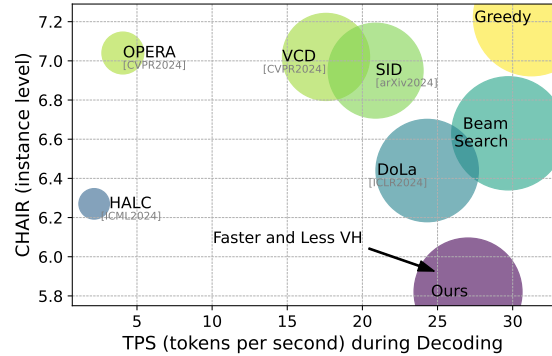


Figure 1. Comparison of decoding speed and hallucination mitigation across methods using LLaVA-1.5 [28] (max new tokens is 64), where a lower instance-level CHAIR score [35] indicates less hallucination and higher TPS during decoding (measured by tokens generated per second) reflects greater decoding efficiency. We present the average of five runs on a single A100 GPU. Comparatively, our approach achieves both lower VH and higher efficiency.

generation through novel model architectures, training methods, and instruction-based data [15, 21, 28, 32, 46, 50]. LVLMs excel at translating complex visual patterns into coherent language representations, leveraging the capabilities of LLMs to significantly enhance visual understanding performance and achieving impressive results across various tasks [2, 13, 27]. However, LVLMs may generate outputs that inaccurately reflect the visual content provided, a phenomenon termed visual hallucinations (VH), which can affect their trustworthiness and suitability in different applications across various domains [17, 24, 26, 31]. Additionally, recent research shows that even advanced and powerful LVLMs remain susceptible to VH [11, 16, 24].

Significant efforts have been directed toward mitigating VH in LVLMs to improve both the reliability and fidelity of their outputs. Existing strategies for reducing VH generally fall into three primary categories: post-processing and self-correction techniques [18, 44, 49], instruction-based fine-tuning [26, 45], and decoding strategy methods [7, 10, 20]. Although the progressive process has been achieved, these

approaches still present several significant limitations, including: (1) a potential dependence on datasets and training, or the addition of complex post-processing steps or high-performing external LVLMs [26, 45, 49]; (2) the necessity for external tools and time-consuming sampling processes for visual localization [7]; (3) multi-round decoding and repeated rollbacks significantly impact decoding speed, diminishing practical usability [18, 20]. As illustrated in Figure 1, such techniques may reduce VH but also compromise efficiency. For instance, state-of-the-art HALC [7] has been shown to reduce the average decoding speed substantially. Consequently, there is an ongoing need for more efficient solutions to mitigate VH while ensuring both efficiency and trustworthiness of LVLMs.

In this work, we present VASparse, an efficient, plug-and-play method for VH mitigation that balances efficiency and trustworthiness from the perspective of visual-aware token sparsity. VASparse is based on several key empirical observations (*cf.* Section 3): (1) the attention of LVLMs exhibits a sparse pattern; (2) directly applying vision-agnostic sparsification methods (e.g., [6, 47]) for token pruning tends to worsen visual fuzziness and exacerbate VH. Based on these insights, VASparse incorporates the following innovative strategies to balance fidelity with efficiency:

**First**, we frame the token sparsification and visual awareness in LVLMs as a unified constrained optimization problem and devise a theoretically optimal token selection strategy during decoding to solve it. **Second**, we introduce a novel sparse-based visual contrastive decoding strategy to reduce hallucinatory tokens. Specifically, we contrast and redistribute the logits generated by visual-agnostic and visual-aware token sparsification to enhance information perception of visual entities, which utilizes embeddings to achieve logits to avoid the time overhead associated with secondary decoding. **Third**, we propose to penalize sinking attention using cumulative attention scores to prevent the model from overfocusing on language-biased or low-semantic tokens.

As illustrated in Figure 1, our VASparse method achieves optimal performance in VH mitigation, with decoding speeds exceeding those of existing VH mitigation methods. Theoretical analysis in Section 4.6 confirms the effectiveness of our visual-aware token selection strategy. Extensive experiments across four popular VH benchmarks and three LVLm families including LLaVA-1.5 [28], MiniGPT-4 [5] and mPLUG-Owl2 [42], demonstrate that VASparse not only delivers superior performance but also achieves competitive decoding speeds (e.g., achieving better performance and up to  $12.9 \times$  speed improvement than HALC [7]).

In summary, our main contributions are threefold:

- We explore VH mitigation from the perspective of token sparsification during decoding and present a novel, efficient, plug-and-play approach that achieves both model fidelity and efficiency, which unifies token sparsity and

visual-aware enhancement as an optimization problem.

- We propose a novel visual-aware token selection strategy, along with a sparse-based visual contrastive decoding method to alleviate VH which utilizes embeddings to achieve contrasted logits and avoids multi-round decoding.
- Comprehensive experiments and evaluations demonstrate that VASparse significantly outperforms existing VH mitigation methods in both performance and decoding speed.

## 2. Related Work

**Large Vision-Language Model.** Recent efforts have attempted to employ LLMs [9, 36–38] as text decoders, combined with visual decoders [33] and a projector, to construct high-performing LVLMs. By integrating visual information with user instructions, LVLMs have achieved significant performance in generating diverse responses and handling complex visual understanding tasks. LLaVA [30] and LLaVA-1.5 [29] integrate pretrained visual encoders and text decoders, leveraging instruction fine-tuning to achieve strong visual understanding performance. InstructBLIP [12] and MiniGPT-4 [51] utilize a Q-former [22] to aggregate multi-modal features, thereby reducing the number of visual tokens required. With optimized architectures, training modes, and diverse data, increasingly advanced LVLm families, such as Qwen-VL [3], mPLUG-Owl2 [43], and InternVL [8], have also been proposed. In this work, we use various architectures of LLaVA-1.5 [29], MiniGPT-4 [51], and mPLUG-Owl2 [43] to evaluate our approach for mitigating VH.

**VH and Evaluation.** LVLMs face challenges from VH which specifically refers to instances where generated content includes inaccurate object descriptions or is unfaithful to the input image information. This phenomenon has been observed in both early BERT-based models [23] and recent LVLMs [32, 46, 50]. In the realm of LVLMs, extensive research has delved into the evaluation and detection of VH [24, 31, 39]. CHAIR [35] is one of the most widely adopted benchmarks for assessing VH. POPE [24] evaluates VH through a binary classification framework, utilizing precision, recall, and accuracy. Furthermore, HALC [7] proposes an offline POPE (OPOPE) to enhance VH evaluation. And MME [14] provides a comprehensive performance assessment of LVLMs with respect to objects, attributes, and other factors. We combine these metrics with decoding speed to comprehensively evaluate the effectiveness of our VASparse in reducing VH while maintaining high efficiency.

**VH Mitigation.** To mitigate VH, various strategies have been developed. Current efforts for reducing VH generally fall into three categories: post-processing techniques [18, 49] and self-correction methods [44]; human feedback-based methods [26, 45]; and decoding strategy approaches [7, 10, 20]. However, the first two strategies may require additional datasets and training or the integration of extra post-processing pipelines or more powerful external

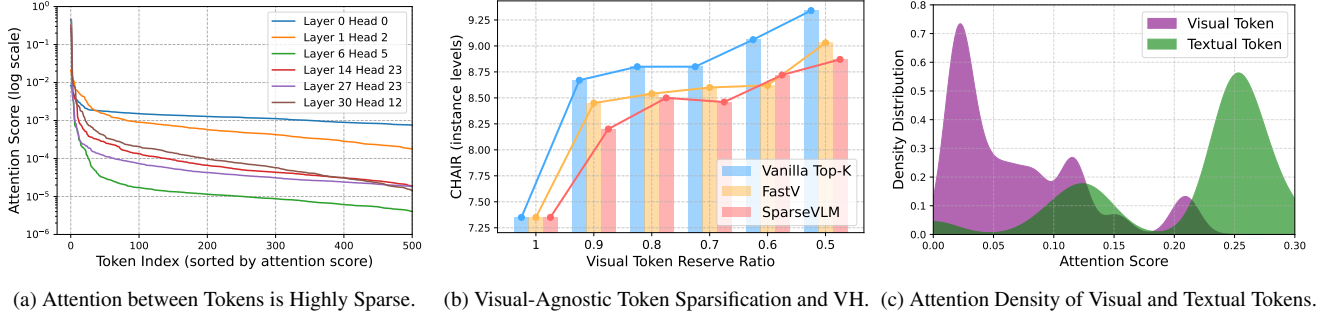


Figure 2. VH evaluation and attention analysis using LLaVA-1.5 on the CHAIR benchmark: (a) token sorting by attention score; (b) token sparsification effects observed with Vanilla Top-K, FastV [6], and SparseVLM [47] on sampled 500 images from the MSCOCO validation set, where Vanilla Top-K denotes keeping tokens with top-K scores in 1-th layer; and (c) attention density distribution across various tokens.

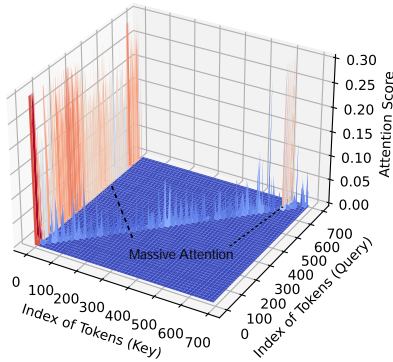


Figure 3. Attention sinking phenomenon in LVLMs: in the 8-th layer and 26-th attention head of LLaVA-1.5, exhibits a substantial concentration of attention on specific tokens, e.g.,  $\langle . \rangle$  and  $\langle s \rangle$ .

LVLMs [26, 45, 49]. The third approach [7, 10, 18–20, 20] primarily explores contrastive decoding strategies based on visual comparisons, which may involve multiple rounds of decoding, time-consuming rollbacks, or even the use of external detection tools. Our work focuses on designing efficient, plug-and-play decoding methods that require no additional training while balancing both performance and efficiency.

### 3. Observation and Motivation

In this section, we present the motivation behind our VAS-parse for mitigating VH. We first provide evidence of attention sparsity in LVLMs and observe that vision-agnostic sparsification methods can intensify VH. Additionally, we emphasize the necessity of attending to image tokens and applying penalties to tokens prone to attention sinking.

#### 3.1. Sparse Activation in LVLm Attention

**Observation:** As shown in Figure 2a, we sort the attention scores calculated for decoding tokens of LVLMs in ascending order. We observe that the attention scores exhibit a clear long-tail distribution, with only a small portion of tokens being heavily activated during decoding. Our results in Fig-

ure 2a indicate that retaining only the top 1% of tokens with the highest attention scores can recall over 98% of the total attention score. This suggests that attention in most layers of the LVLm decoder is sparse.

**Insights:** Our findings substantiate that self-attention in most layers of the LVLm decoder is sparse. This insight suggests the potential for pruning corresponding tokens to reduce computational cost during decoding.

#### 3.2. Vision-Agnostic Sparsification Aggravates VH

**Observation:** Given the sparsity of attention in LVLMs, we evaluate VH with vision-agnostic (do not adjust token selection during decoding) token sparsification, including the vanilla Top-K strategy, FastV [6] and SparseVLM [47]. As shown in Figure 2b, we observe that as the level of sparsification increases, the model becomes more prone to VH.

**Insights:** Our empirical findings indicate that these vision-agnostic sparsification techniques exacerbate VH in LVLMs, suggesting that merely applying such methods to speed up decoding may undermine output trustworthiness.

#### 3.3. Distinct Distribution of Image and Text Tokens

**Observation:** We analyze the attention distribution of visual and textual tokens, with the results shown in Figure 2c. A clear divergence in distribution is evident: image tokens predominantly occupy lower-attention regions, whereas text tokens concentrate in higher-attention regions.

**Insights:** These findings suggest that LVLMs tend to prioritize text tokens over image tokens during decoding. This explains why vision-agnostic token sparsification strategies may worsen hallucinations (*cf.* Section 3.2): they are more likely to prune low-attention image tokens, which may contain crucial visual information. This insight highlights the potential benefits of improving the model’s awareness of image tokens during sparsification.

#### 3.4. Attention Sinking on Textual Tokens

**Observation:** We further analyzed the attention patterns in LVLMs and observed a significant attention “sink” effect [18,

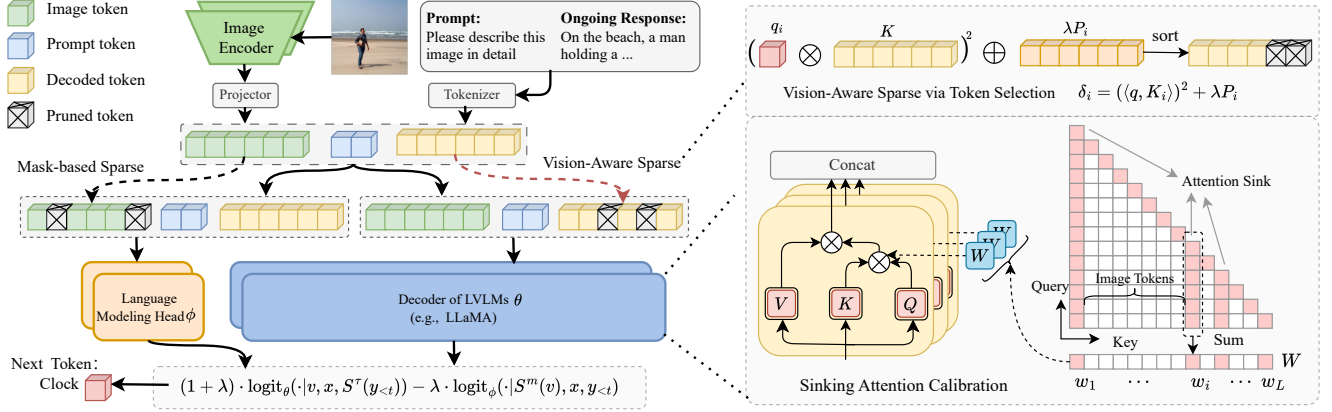


Figure 4. The illustration of the proposed VASparse framework, which consists of (1) the visual-aware token selection designed to prune the generated tokens during decoding; (2) a sparse-based visual contrastive decoding method to recalibrate the distribution of hallucinated outputs; and (3) the calibration strategy for punishing sinking attention.

41] in certain text tokens (as illustrated in Figure 3). This phenomenon resembles the summary token and attention bias effects observed in LLMs [41]. However, distinct from LLMs, our findings indicate that in LVLMs, attention sink tokens are primarily concentrated in text tokens, even when text tokens are vastly outnumbered by image tokens. Notably, these attention sink tokens are typically low in semantic content, such as  $\langle . \rangle$  and  $\langle s \rangle$ .

**Insights:** Tokens with attention sinking in LVLMs exhibit high attention and low semantic information. This pattern suggests an intrinsic bias within LVLMs. However, excessive focus on low-semantic tokens may cause the model to rely heavily on linguistic priors and neglect visual information. Therefore, applying penalties to these sinking tokens could enhance the LVLm’s perception of visual tokens.

## 4. Methodology

### 4.1. Preliminaries

We consider a general LVLm  $\theta$ , which integrates a vision encoder, a vision-text interface, and a decoder of LLM. Initially, the image  $v$  undergoes processing through the vision encoder to produce embeddings, which are then modified by the interface (e.g., linear layer and Q-Former [22]) to align with the query  $x$ . The combined data serves as input to the decoder, which autoregressively generates the output  $y$  as:

$$y_t \sim p_\theta(y_t | v, x, y_{<t}) \propto \exp(\text{logit}_\theta(y_t | v, x, y_{<t})), \quad (1)$$

where  $y_t$  represents the  $t$ -th token of  $y$ , and  $y_{<t}$  refers to the sequence of tokens generated prior to the  $t$ -th step. The function  $\text{logit}_\theta$  is the logit distribution function.

During decoding, the key  $K$  and value  $V$  within the attention head are derived from preceding decoding steps and stored in a key-value cache to avoid redundant computations.

Consequently, the attention with dimension  $D$  for decoding the  $t$ -th token proceeds during decoding as follows:

$$\text{Attention}(q_t, K_{\leq t}) = \text{Softmax}\left(\frac{q_t K_{\leq t}^\top}{\sqrt{D}}\right), \quad (2)$$

where  $q_t$  is the query for the current decoding step, and  $K_{\leq t}$  represents the keys up to and including step  $t$ .

Our primary goal is to reduce generated hallucinatory tokens to preserve the trustworthiness of the generated text and maintain efficient decoding speed.

### 4.2. Problem Formulation

Building on our observations in Section 3, we decompose the unified objective of achieving both trustworthiness and efficiency for LVLMs into the following sub-goals:

**Goal 1 (Token Sparsification):** Given the sparsity of LVLMs (cf. Section 3.1), we define token sparsification through a binary mask  $M$ , where each element  $M_i \in \{0, 1\}$ . Optimal sparsification minimizes  $\sum_{i=1}^L M_i$  while maximizing the recall of attention scores, aiming for  $q(M \odot K)^\top$  to approximate the full attention score  $qK^\top$  as closely as possible, where  $L$  is the generated sequence length and  $M_i = 0$  indicates that the token  $K_i$  will be pruned during decoding.

**Goal 2 (Vision-Aware Decoding):** During decoding, some tokens may hold lower attention scores but are crucial for decoding visually relevant instances. Ignoring these tokens can exacerbate VH (cf. Section 3.2 and 3.3). We assign each token a vision-aware saliency score  $P_i$  to represent its importance for decoding visual instances. A higher  $P_i$  indicates that the token should be more likely to be retained.

The above objectives can be summarized as maintaining the original attention scores as much as possible while sparsifying the tokens and considering visual information during the decoding process. We innovatively unify these

optimization goals into a constrained optimization problem which minimizes the error between the recalled attention scores and the full attention scores:

**Definition 1 (Unified Objective):** We define the joint objective of trustworthiness and efficiency in LVLMs as the solution to the following constrained optimization problem:

$$\begin{aligned} \min_M \quad & \mathcal{E}(M) = \|qK^\top - q(M \odot K)^\top\|^2 - \lambda P \cdot M \\ & = \sum_{i=1}^L (\langle q, K_i \rangle - M_i \langle q, K_i \rangle)^2 - \lambda P_i \cdot M_i \quad (3) \\ \text{s.t.} \quad & M_i \in \{0, 1\}, \forall i = 1, 2, \dots, L; \quad \sum_{i=1}^L M_i = S, \end{aligned}$$

where,  $q \in \mathbb{R}^{1 \times D}$ ,  $K_i \in K$  and  $K_i \in \mathbb{R}^{1 \times D}$ ,  $\|\cdot\|^2$  represents the  $L_2$  norm.  $\langle \cdot, \cdot \rangle$  denotes the inner product, and  $S$  is the sparsity rate, and  $\lambda$  is a tradeoff parameter used to balance visual perception and attention recall.

The objective 1 inherently includes the following constraints: (1) Sparsity Constraint:  $\sum_{i=1}^L M_i = S$ , and  $S$  denotes the number of non-zero elements in  $M$ , with  $S < L$  and  $M_i \in \{0, 1\}$ ; (2) Visual Saliency Constraint:  $P = \{P_i\}_{i=1}^L$  represents the visual-aware scores. To solve this problem 1 efficiently, we propose a novel **visual-aware token selection strategy** to achieve efficient VH mitigation as the overall framework shown in Figure 4.

### 4.3. Visual-Aware Token Selection

To solve the unified objective (Def. 1) and mitigate VH efficiently, we propose a visual-aware token selection strategy. Specifically, for each attention head, we rank tokens based on an aggregated score  $\delta_i$  in descending order, and setting  $M_i = 1$  for the top- $S$  tokens and  $M_i = 0$  for the rest. The proposed aggregation score  $\delta_i$  for each token is defined as:

$$\delta_i = (\langle q, K_i \rangle)^2 + \lambda P_i, \quad (4)$$

where,  $\langle \cdot, \cdot \rangle$  denotes the inner product, the score  $\delta_i$  combines both the attention score  $\langle q, K \rangle$  and the visual saliency  $P_i$ , ensuring that the visually relevant tokens are retained while preserving computational efficiency.

To obtain visual-aware scores (Goal 2 in Section 4.2), we utilize the attention scores of each generated token and the image tokens, which are treated as the visual saliency scores for the respective tokens. Specifically, we compute the visual saliency score  $P$  by retaining the weights from the last attention head in the LVLM’s historical calculations:

$$P_i = \frac{\exp\left(\sum_{k \in \mathcal{I}(v)} a_{i,k}\right)}{\sum_j \exp\left(\sum_{k \in \mathcal{I}(v)} a_{j,k}\right)}, \quad (5)$$

where  $\mathcal{I}(v)$  represents the set of image tokens and  $a_{i,j}$  is the attention score between tokens  $i$  and  $j$ .

By using the image token attention scores as a measure of significance, we can effectively leverage the attention weights already computed, while avoiding the introduction of additional computational overhead. For the discarded token set  $\mathcal{T} = \{K_i \mid M_i = 0\}$ , we employ the  $k$ -nearest neighbor density peak aggregation algorithm [34] to achieve adaptive token aggregation. Tokens within the same cluster are summed and retained as a single aggregated token.

### 4.4. Sparse-based Visual Contrastive Decoding

Based on our empirical observations, we can leverage the finding that vision-agnostic token sparsification intensifies VH to mitigate language bias in the output distribution. We innovatively propose to amplify the informational contrast within the visual context by redistributing logits in the output by contrasting the decoding probability distributions of vision-aware and vision-agnostic (mask-based) sparsifications  $S^\tau$  and  $S^m$ . However, directly using the output distribution from LVLMs to obtain the contrastive logit distribution would inevitably incur significant overhead due to the secondary decoding process. To address this, we propose using only the embeddings of vision-agnostic tokens as input to the language decoding head  $\phi$  of the LLM decoder to obtain the logit distribution, without going through the full text decoder. Specifically, we adopt the proposed visual-aware sparsification strategy (cf. Section 4.3) to obtain the logit distribution  $\text{logit}_\theta$ . Then, we randomly mask the visual tokens and input their embeddings directly into the language decoding head of the LLM to obtain the contrastive logit distribution  $\text{logit}_\phi$ . Finally, we assign the logit distributions of the tokens to obtain the final results:

$$\begin{aligned} y_t \sim & (1 + \alpha) \cdot \text{logit}_\theta(\cdot \mid v, x, S^\tau(y_{<t})) \\ & - \alpha \cdot \text{logit}_\phi(\cdot \mid S^m(v), x, y_{<t}), \quad (6) \end{aligned}$$

where,  $\alpha$  is a trade-off. Note that our decoding strategy bypasses the LVLM’s decoder (e.g., a LLaMA2-7B [38]), thereby avoiding the secondary computational overhead. Inspired by [20], we apply adaptive plausibility constraints to our sparse-based visual contrastive decoding.

### 4.5. Sinking Attention Penalty

Our observations (cf. Section 3.4) indicate a pronounced attention sinking in LVLMs, where tokens receive disproportionately high attention scores despite low semantic information. Excessive focus on such tokens can blur visual information during decoding. Therefore, a targeted penalty should be applied to tokens exhibiting abnormally high attention scores. We define a penalty weight matrix  $W = \{w_1, \dots, w_L\}$ , where each  $w_i$  serves as a penalty factor for anomalous attention scores. To efficiently implement the penalty for sinking attention, we accumulate the attention

Methods	LLaVA-1.5			MiniGPT-4			mPLUG-Owl2		
	CHAIR <sub>i</sub> ↓	CHAIR <sub>s</sub> ↓	TPS↑	CHAIR <sub>i</sub> ↓	CHAIR <sub>s</sub> ↓	TPS↑	CHAIR <sub>i</sub> ↓	CHAIR <sub>s</sub> ↓	TPS↑
FastV*	8.53	26.76	33.21	16.72	41.32	38.29	11.40	38.49	24.6
SparseVLM*	8.44	26.11	32.47	16.38	40.93	37.81	11.35	38.99	23.73
Woodpecker†	6.72	19.79	-	12.09	31.69	-	8.99	25.05	-
LURE†	6.67	19.75	-	11.80	31.67	-	7.78	22.53	-
Greedy	7.22	22.20	31.25	12.17	31.47	36.64	8.94	24.42	20.36
Beam Search	6.43	19.97	29.91	11.57	31.80	32.27	8.72	23.87	19.62
OPERA	7.04	21.28	4.36	12.34	32.63	5.57	9.07	24.48	3.56
VCD	7.02	21.40	17.58	11.90	30.60	17.69	9.13	24.89	9.89
DoLa	6.44	20.23	23.61	11.62	30.58	25.01	8.88	24.67	14.74
SID	6.95	20.83	20.88	11.85	31.73	22.95	8.54	23.55	12.95
HALC	6.27	19.64	2.15	11.69	31.76	3.86	7.71	23.48	1.52
Ours	<b>5.82</b>	<b>18.51</b>	27.73	<b>11.35</b>	<b>30.19</b>	30.87	<b>7.36</b>	<b>22.03</b>	18.18

Table 1. Comparison of the average CHAIR evaluation results (instance levels CHAIR<sub>i</sub> and sentence levels CHAIR<sub>s</sub>) and token per second (TPS) during decoding with different baselines on MSCOCO datasets of five random runs, with whole statistical results in Appendix. \* represents the image token sparsity method and † is the post-hoc methods.

scores of each token with subsequent queries to evaluate the degree of sinking. We then apply *softmax* normalization to obtain a calibration weight for sinking attention:

$$w_j = \frac{\exp\left(\sum_{i=j}^L a_{i,j}\right)}{\sum_{k=1}^L \exp\left(\sum_{i=k}^L a_{i,k}\right)}, \quad (7)$$

where  $a_{i,j}$  denotes the element in the  $i$ -th row and  $j$ -th column of the attention matrix, and  $w_j$  represents the  $j$ -th element of the weight vector  $W$  after applying the *softmax* operation. This approach ensures that sinking attention is evaluated progressively across subsequent queries, and  $W$  will be utilized as a weight as  $(1 + \beta)qK^\top - \beta W \odot qK^\top$  during decoding, as shown in Figure 4.

#### 4.6. Theoretical Analysis

**Theorem 1 (Global Optimality):** *By employing the selection strategy defined in Section 4.3, we can obtain a globally optimal solution for the optimization problem defined in Def. 1. Specifically, the sparse mask  $M$  derived from this selection strategy satisfies:*

$$M^* = \arg \min_M \mathcal{E}(M). \quad (8)$$

**Intuition:** The proof and more analysis of the theorem 1 is provided in the Appendix. This theorem ensures that the proposed token selection strategy yields the minimum error  $\mathcal{E}(M)$ . This theoretical analysis further validates the effectiveness of the proposed VASparse in achieving both token sparsification and efficient visual perception.

## 5. Experiments

**Benchmarks.** Following common settings [7, 20, 44], We evaluate the effectiveness of our VASparse in VH mit-

igation on four popular benchmarks: (1) quantitative metrics CHAIR [35] on MSCOCO dataset [25]; (2) the offline Polling-based Object Probing Evaluation (POPE) [7, 24] on the MSCOCO dataset; (3) general-purposed Multimodal Large Language Model Evaluation (MME) benchmark [14]; (4) GPT-4 assisted benchmark [48] relies on the advanced GPT-4 to judge the fine-grained VH and calculate Sentence-level Hallucination Ratio (SHR).

**Baselines.** We compare our VASparse with greedy decoding and beam search decoding, and various state-of-the-art (SOTA) decoding methods as baselines, including DoLa [10], OPERA [18], VCD [20], SID [19] and HALC [7]. We also compare the post-processing VH elimination method (i.e., Woodpecker [44], LURE [49]) with some token sparsity methods (i.e., FastV [6] and SparseVLMs [47]).

**Backbones.** Following previous settings [7, 20], we select popular LVLMS families, e.g., LLaVA-1.5 [28], MiniGPT-4 [5] and mPLUG-Owl2 [42] as the base modal for all baselines except Woodpecker and LURE, where, Woodpecker and LURE utilize extra LLMs, i.e., ChatGPT [4] and GPT-4 [1], for self-correction and distillation. We investigate the VH of these LVLMS under different decoding to evaluate the effectiveness of our VASparse.

**Settings.** We implement the proposed VASparse based on HuggingFace Transformers [40] and combine it with beam search for decoding. We evaluate settings with maximum generation lengths  $L_{max}$  of 64 and 512. When  $L_{max}$  is 64, the beam size is set to 3, and for  $L_{max} = 512$ , it is set to 2. The sparsity rate top- $S$  is set to 0.9 times  $L$ , and the image masking sparsity rate for  $S^m$  is set to 0.5. The hyperparameter  $\lambda$  in Eq. 4,  $\alpha$  in Eq. 6 and  $\beta$  in Section 4.5 are set to 0.1. The decoding process of LVLMS and all experiments are performed on 8 A100 GPUs. For token sparsity methods, we retain 75% of tokens during inference. Other methods

Methods	LLaVA-1.5			MiniGPT-4			mPLUG-Owl2		
	Random	Popular	Adversarial	Random	Popular	Adversarial	Random	Popular	Adversarial
Woodpecker <sup>†</sup>	59.73	58.53	58.07	53.84	51.70	51.27	58.10	53.07	55.42
LURE <sup>†</sup>	60.08	58.63	58.34	53.91	52.37	51.38	58.28	53.15	55.65
Greedy	58.75	57.42	56.64	53.71	51.68	51.92	57.40	53.43	55.43
Beam Search	60.38	58.98	58.43	53.97	52.27	51.93	55.31	52.89	53.12
OPERA	59.80	58.42	58.00	53.08	51.32	51.20	55.70	53.41	53.66
VCD	60.05	58.34	58.02	53.26	51.50	51.07	<b>58.63</b>	54.87	56.13
DoLa	59.36	58.08	57.44	53.83	51.93	51.72	57.21	53.38	55.24
SID	61.63	59.62	58.83	53.86	51.98	51.77	55.82	53.46	56.07
HALC	60.46	59.33	58.50	53.93	52.06	51.80	56.29	53.38	55.84
Ours	<b>62.13</b>	<b>60.93</b>	<b>59.20</b>	<b>54.87</b>	<b>52.93</b>	<b>52.70</b>	58.27	<b>55.28</b>	<b>56.77</b>

Table 2. Comparison of the average F1-score evaluation results under different settings (i.e., *Random*, *Popular*, *Adversarial*) with different baselines and our VASparse on offline POPE benchmark [7, 24] of five random runs, with whole statistical results in Appendix. Higher F1-score indicate better performance and bold indicates the best results. † denotes the post-hoc method.

Methods	LLaVA-1.5				MiniGPT-4				mPLUG-Owl2			
	Object-level <sup>↑</sup>		Attribute-level <sup>↑</sup>		Object-level <sup>↑</sup>		Attribute-level <sup>↑</sup>		Object-level <sup>↑</sup>		Attribute-level <sup>↑</sup>	
	Existence	Count	Position	Color	Existence	Count	Position	Color	Existence	Count	Position	Color
Greedy	165.67	120.00	110.67	148.33	137.00	93.00	75.00	125.00	167.00	120.00	105.00	145.00
DoLa	170.00	120.00	106.67	150.67	137.00	90.00	75.33	122.67	167.00	125.00	110.00	147.67
OPERA	165.00	115.67	104.00	145.00	140.67	92.33	73.00	125.00	167.00	122.33	100.00	145.00
VCD	175.33	130.33	115.00	155.00	142.00	95.33	71.33	129.00	171.33	125.00	107.33	150.00
HALC	167.67	121.33	106.67	150.67	140.00	92.67	71.33	122.67	167.00	120.33	108.67	145.00
Ours	<b>180.00</b>	<b>132.67</b>	<b>121.33</b>	<b>160.00</b>	<b>147.33</b>	<b>98.67</b>	<b>78.67</b>	<b>133.00</b>	<b>175.00</b>	<b>130.00</b>	<b>110.67</b>	<b>155.00</b>

Table 3. Results on the subset of the MME benchmark for evaluating object-level and attribute-level VH, where the best performances within each setting are bolded. We randomly run it five times to obtain the average result, with the whole statistical results in Appendix.

use the settings as described in original papers. More details and results under  $L_{max} = 512$  are provided in Appendix.

## 5.1. Main Results

**CHAIR Evaluation.** Following HALC [7], we set ‘*Please describe this image in detail.*’ as the input prompt and utilize generated tokens per second (TPS) to evaluate the efficiency, as results are shown in Table 1. Based on the results, we have several detailed observations: (1) It can be observed that our method significantly outperforms existing decoding and post-processing baselines for reducing VH. Our VASparse achieved the lowest VH rate at both the sentence and instance levels across three families of LVLMs, which demonstrates the superiority and generalizability of our method in alleviating VH. (2) Compared to SOTA decoding methods, VASparse maintains competitive decoding speed without secondary decoding or reprocessing via extra LLMs, e.g., achieving speeds that are  $12.9\times$  and  $6.4\times$  faster than HALC [7] and OPERA [18], respectively. (3) Although the sparsification method accelerates the inference speed, it exacerbates visual ambiguity, which in turn aggravates VH.

**POPE Evaluation.** Following HALC [7], we utilize offline POPE (OPOPE) benchmark with F1-score as metrics to evaluate VH, which replaces the live interactions of POPE with offline checks. As shown in Table 2, we have several observations: (1) VASparse consistently achieves optimal results in most settings, outperforming both SOTA decoding methods and post-processing methods. This further demonstrates the effectiveness of VASparse; (2) VASparse effectively mitigates VH across three different LVLM architectures, demonstrating the versatility and plug-and-play nature.

**MME Benchmarks.** Following [7, 20, 44], we adopt object-level subsets (“existence” and “count”) and attribute-level subsets (“position” and “color”) of MME benchmark [14] to evaluate VH. As shown in Table 3, we can observe that: (1) Our VASparse can significantly reduce object and attribute hallucination, and achieve optimal VH mitigation performance. (2) HALC and OPERA do not exhibit significant VH mitigation on the MME benchmark. This is because the MME evaluation is designed as a binary classification task, requiring LVLMs to output only a few tokens, which limits the effectiveness of methods that need to decode sequences

G. Settings		LLaVA-1.5			MiniGPT-4		
		CHAIR <sub>i</sub> ↓	CHAIR <sub>s</sub> ↓	TPS ↑	CHAIR <sub>i</sub> ↓	CHAIR <sub>s</sub> ↓	TPS ↑
1	w/o Whole Visual-Aware Token Selection (i.e., Eq. 4)	6.43	19.75	25.54	11.63	30.51	27.55
	w/o Visual Perception Score $P$ in Eq. 4	6.06	19.20	27.80	11.57	31.05	30.96
2	w/o Whole SVCD (i.e., Eq. 6)	6.91	21.42	<b>30.68</b>	11.85	30.93	<b>35.83</b>
	w/o Mask-based Sparsification $S^m$ in Eq. 6	6.31	18.85	27.47	11.58	31.26	30.30
3	w/o Sinking Attention Penalty (i.e., Eq. 7)	6.32	19.39	27.96	11.52	31.04	30.92
4	Our Full VASparse	<b>5.82</b>	<b>18.51</b>	27.73	<b>11.35</b>	<b>30.19</b>	30.87

Table 4. Ablation experiments on the CHAIR benchmark, with the best results highlighted in bold and the whole results in Appendix.

Methods	LLaVA-1.5	MiniGPT-4	mPLUG-Owl2
Greedy	36.3	46.7	42.3
OPERA	34.2	45.9	41.7
VCD	34.6	46.0	41.9
HALC	33.9	45.8	41.7
Ours	<b>33.5</b>	<b>45.2</b>	<b>41.1</b>

Table 5. Performance (SHR) comparison on GPT-4 assisted benchmark, where, the lower value denotes the lower VH.

of a certain length and handle special entity tokens.

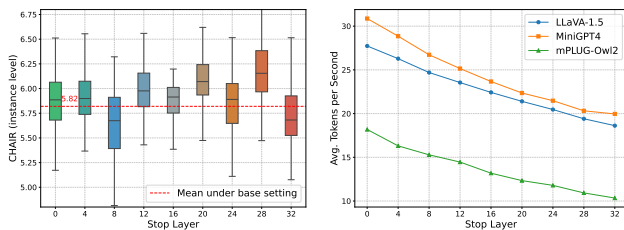
**GPT-4 Assisted Benchmarks.** We conduct experiments on the GPT-4 assisted benchmark to evaluate the fine-grained VH of different methods, and the results are presented in Table 5. We can observe that our VASparse achieved the best SHR metric among the four LVLMS, which further confirms the superiority of our method in mitigating VH.

## 5.2. Method Analysis

We conduct ablation experiments using CHAIR on MSCOCO to evaluate the effectiveness of the components of our proposed VASparse in detail. Specifically, we evaluate the effectiveness of the components by removing or modifying the specific settings as results shown in Table 5.

**Effect of the Visual-Aware Token Selection.** As shown in Groups 1 and 4 in Table 4, removing the whole visual-aware token selection strategy leads to a performance decrease and reduces decoding speed. This suggests that sparsifying the model’s decoding sequence to some extent can mitigate the language bias in LVLMS and reduce the involvement of certain tokens in attention computation. Moreover, removing the visual perception score also results in a performance decline. These results consistently demonstrate the effectiveness of our visual-aware token selection strategy.

**Effect of the Sparse-based Visual Contrastive Decoding.** To evaluate the effectiveness of our sparse-based visual contrastive decoding (SVCD), we remove both the full SVCD and the mask-based sparsification  $S^m$  in Eq. 6. As shown in Groups 2 and 4 of Table 4, we observe a significant performance decline, which further validates the effectiveness of our SVCD and mask-based sparsification strategy.



(a) CHAIR<sub>i</sub> evaluation results.

(b) TPS during decoding.

Figure 5. Performance and efficiency analysis of different logit sources: (a) the impact of using different early stopping layers on LLaVA-1.5 performance; (b) the impact of using different early stopping layers on decoding speeds (TPS).

**Effect of the Sinking Attention Calibration.** Moreover, we removed the calibration mechanism for the sinking attention, and observed a further decline in the method’s VH mitigation effect. This further demonstrates the relevance of sinking attention to VH and the effectiveness of the proposed attention calibration strategy.

**Decoding Efficiency Analysis.** To further validate the effect of using embedding features to compute the proposed SVCD, we calculate the contrastive logits from features at different depths of the LVLMS decoder to calibrate the distribution, and observe performance and decoding speed, as shown in Figure 5. We observe that by using only embedded features (i.e., stop layer is 0), our method already achieves good VH mitigation performance while attaining optimal decoding speed. In this way, our VASparse effectively avoids the time-consuming secondary decoding process, achieving a balance between performance and efficiency.

## 6. Conclusion

This work proposes an efficient, plug-and-play decoding strategy, VASparse, to mitigate VH in LVLMS. Inspired by the sparse activation pattern of LVLMS and the role of visual-agnostic token sparsification in worsening VH, we propose a visual-aware token selection strategy during decoding. Subsequently, we innovatively introduce sparse-based visual contrastive decoding to recalibrate the logits without secondary decoding, and adjust sinking attention. Extensive



experiments show the effectiveness of VASparse in reducing VH across various benchmarks and LVLm families.

## References

- [1] OpenAI Josh Achiam and et al. Steven Adler. Gpt-4 technical report. 2023. 6
- [2] Jinze Bai, Shuai Bai, Shusheng Yang, Shijie Wang, Sinan Tan, Peng Wang, Junyang Lin, Chang Zhou, and Jingren Zhou. Qwen-vl: A frontier large vision-language model with versatile abilities. *ArXiv*, abs/2308.12966, 2023. 1
- [3] Jinze Bai, Shuai Bai, Shusheng Yang, Shijie Wang, Sinan Tan, Peng Wang, Junyang Lin, Chang Zhou, and Jingren Zhou. Qwen-vl: A frontier large vision-language model with versatile abilities. *arXiv preprint arXiv:2308.12966*, 2023. 2
- [4] Tom B. Brown, Benjamin Mann, Nick Ryder, Melanie Subbiah, Jared Kaplan, Prafulla Dhariwal, Arvind Neelakantan, Pranav Shyam, Girish Sastry, Amanda Askell, Sandhini Agarwal, Ariel Herbert-Voss, Gretchen Krueger, Tom Henighan, Rewon Child, Aditya Ramesh, Daniel M. Ziegler, Jeff Wu, Clemens Winter, Christopher Hesse, Mark Chen, Eric Sigler, Mateusz Litwin, Scott Gray, Benjamin Chess, Jack Clark, Christopher Berner, Sam McCandlish, Alec Radford, Ilya Sutskever, and Dario Amodei. Language models are few-shot learners. *ArXiv*, abs/2005.14165, 2020. 6
- [5] Jun Chen, Deyao Zhu, Xiaoqian Shen, Xiang Li, Zechun Liu, Pengchuan Zhang, Raghuraman Krishnamoorthi, Vikas Chandra, Yunyang Xiong, and Mohamed Elhoseiny. Minigt-v2: large language model as a unified interface for vision-language multi-task learning. *ArXiv*, abs/2310.09478, 2023. 2, 6
- [6] Liang Chen, Haozhe Zhao, Tianyu Liu, Shuai Bai, Junyang Lin, Chang Zhou, and Baobao Chang. An image is worth 1/2 tokens after layer 2: Plug-and-play inference acceleration for large vision-language models, 2024. 2, 3, 6, 12
- [7] Zhaorun Chen, Zhaorun Chen, Zhuokai Zhao, Hongyin Luo, Huaxiu Yao, Bo Li, and Jiawei Zhou. Halc: Object hallucination reduction via adaptive focal-contrast decoding. *ArXiv*, abs/2403.00425, 2024. 1, 2, 3, 6, 7, 12, 13, 14, 15, 16
- [8] Zhe Chen, Jiannan Wu, Wenhai Wang, Weijie Su, Guo Chen, Sen Xing, Muyan Zhong, Qinglong Zhang, Xizhou Zhu, Lewei Lu, et al. Internvl: Scaling up vision foundation models and aligning for generic visual-linguistic tasks. In *Proceedings of the IEEE/CVF Conference on Computer Vision and Pattern Recognition*, pages 24185–24198, 2024. 2
- [9] Wei-Lin Chiang, Zhuohan Li, Zi Lin, Ying Sheng, Zhanghao Wu, Hao Zhang, Lianmin Zheng, Siyuan Zhuang, Yonghao Zhuang, Joseph E Gonzalez, et al. Vicuna: An open-source chatbot impressing gpt-4 with 90%\* chatgpt quality. See <https://vicuna.lmsys.org> (accessed 14 April 2023), 2(3):6, 2023. 2
- [10] Yung-Sung Chuang, Yujia Xie, Hongyin Luo, Yoon Kim, James R. Glass, and Pengcheng He. Dola: Decoding by contrasting layers improves factuality in large language models. *ArXiv*, abs/2309.03883, 2023. 1, 2, 3, 6, 12
- [11] Wenliang Dai, Zihan Liu, Ziwei Ji, Dan Su, and Pascale Fung. Plausible may not be faithful: Probing object hallucination in vision-language pre-training. *ArXiv*, abs/2210.07688, 2022. 1
- [12] Wenliang Dai, Junnan Li, Dongxu Li, Anthony Meng Huat Tiong, Junqi Zhao, Weisheng Wang, Boyang Li, Pascale Fung, and Steven Hoi. Instructblip: Towards general-purpose vision-language models with instruction tuning, 2023. 2
- [13] Wenliang Dai, Junnan Li, Dongxu Li, Anthony Meng Huat Tiong, Junqi Zhao, Weisheng Wang, Boyang Albert Li, Pascale Fung, and Steven C. H. Hoi. Instructblip: Towards general-purpose vision-language models with instruction tuning. *ArXiv*, abs/2305.06500, 2023. 1
- [14] Chaoyou Fu, Peixian Chen, Yunhang Shen, Yulei Qin, Mengdan Zhang, Xu Lin, Zhenyu Qiu, Wei Lin, Jinrui Yang, Xiawu Zheng, Ke Li, Xing Sun, and Rongrong Ji. Mme: A comprehensive evaluation benchmark for multimodal large language models. *ArXiv*, abs/2306.13394, 2023. 2, 6, 7
- [15] Tao Gong, Chengqi Lyu, Shilong Zhang, Yudong Wang, Miao Zheng, Qianmengke Zhao, Kuikun Liu, Wenwei Zhang, Ping Luo, and Kai Chen. Multimodal-gpt: A vision and language model for dialogue with humans. *ArXiv*, abs/2305.04790, 2023. 1
- [16] Tianrui Guan, Fuxiao Liu, Xiyang Wu, Ruiqi Xian, Zongxia Li, Xiaoyu Liu, Xijun Wang, Lichang Chen, Furong Huang, Yaser Yacoob, Dinesh Manocha, and Tianyi Zhou. Hallusion-bench: An advanced diagnostic suite for entangled language hallucination and visual illusion in large vision-language models. 2023. 1
- [17] Anish Gunjal, Jihan Yin, and Erhan Bas. Detecting and preventing hallucinations in large vision language models. In *AAAI Conference on Artificial Intelligence*, 2023. 1
- [18] Qidong Huang, Xiao wen Dong, Pan Zhang, Bin Wang, Conghui He, Jiaqi Wang, Dahua Lin, Weiming Zhang, and Neng H. Yu. Opera: Alleviating hallucination in multimodal large language models via over-trust penalty and retrospection-allocation. *ArXiv*, abs/2311.17911, 2023. 1, 2, 3, 6, 7, 12
- [19] Fushuo Huo, Wenchao Xu, Zhong Zhang, Haozhao Wang, Zhicheng Chen, and Peilin Zhao. Self-introspective decoding: Alleviating hallucinations for large vision-language models, 2024. 6, 12
- [20] Sicong Leng, Hang Zhang, Guanzheng Chen, Xin Li, Shijian Lu, Chunyan Miao, and Li Bing. Mitigating object hallucinations in large vision-language models through visual contrastive decoding. *ArXiv*, abs/2311.16922, 2023. 1, 2, 3, 5, 6, 7, 12, 14
- [21] Bo Li, Yuanhan Zhang, Liangyu Chen, Jinghao Wang, Jingkang Yang, and Ziwei Liu. Otter: A multi-modal model with in-context instruction tuning. *ArXiv*, abs/2305.03726, 2023. 1
- [22] Junnan Li, Dongxu Li, Silvio Savarese, and Steven Hoi. Blip-2: Bootstrapping language-image pre-training with frozen image encoders and large language models. In *International conference on machine learning*, pages 19730–19742. PMLR, 2023. 2, 4
- [23] Liunian Harold Li, Mark Yatskar, Da Yin, Cho-Jui Hsieh, and Kai-Wei Chang. Visualbert: A simple and performant baseline for vision and language. *ArXiv*, abs/1908.03557, 2019. 2

- [24] Yifan Li, Yifan Du, Kun Zhou, Jinpeng Wang, Wayne Xin Zhao, and Ji rong Wen. Evaluating object hallucination in large vision-language models. In *Conference on Empirical Methods in Natural Language Processing*, 2023. 1, 2, 6, 7, 15, 16
- [25] Tsung-Yi Lin, Michael Maire, Serge J. Belongie, James Hays, Pietro Perona, Deva Ramanan, Piotr Dollár, and C. Lawrence Zitnick. Microsoft coco: Common objects in context. In *European Conference on Computer Vision*, 2014. 6
- [26] Fuxiao Liu, Kevin Lin, Linjie Li, Jianfeng Wang, Yaser Yacoob, and Lijuan Wang. Mitigating hallucination in large multi-modal models via robust instruction tuning. 2023. 1, 2, 3
- [27] Haotian Liu, Chunyuan Li, Yuheng Li, and Yong Jae Lee. Improved baselines with visual instruction tuning. *ArXiv*, abs/2310.03744, 2023. 1, 14
- [28] Haotian Liu, Chunyuan Li, Qingyang Wu, and Yong Jae Lee. Visual instruction tuning. *ArXiv*, abs/2304.08485, 2023. 1, 2, 6
- [29] Haotian Liu, Chunyuan Li, Yuheng Li, and Yong Jae Lee. Improved baselines with visual instruction tuning. In *Proceedings of the IEEE/CVF Conference on Computer Vision and Pattern Recognition*, pages 26296–26306, 2024. 2
- [30] Haotian Liu, Chunyuan Li, Qingyang Wu, and Yong Jae Lee. Visual instruction tuning. *Advances in neural information processing systems*, 36, 2024. 2
- [31] Holy Lovenia, Wenliang Dai, Samuel Cahyawijaya, Ziwei Ji, and Pascale Fung. Negative object presence evaluation (nope) to measure object hallucination in vision-language models. *ArXiv*, abs/2310.05338, 2023. 1, 2
- [32] Muhammad Maaz, Hanoona Abdul Rasheed, Salman H. Khan, and Fahad Shahbaz Khan. Video-chatgpt: Towards detailed video understanding via large vision and language models. *ArXiv*, abs/2306.05424, 2023. 1, 2
- [33] Alec Radford, Jong Wook Kim, Chris Hallacy, Aditya Ramesh, Gabriel Goh, Sandhini Agarwal, Girish Sastry, Amanda Askell, Pamela Mishkin, Jack Clark, Gretchen Krueger, and Ilya Sutskever. Learning transferable visual models from natural language supervision, 2021. 2
- [34] Alex Rodriguez and Alessandro Laio. Clustering by fast search and find of density peaks. *science*, 344(6191):1492–1496, 2014. 5
- [35] Anna Rohrbach, Lisa Anne Hendricks, Kaylee Burns, Trevor Darrell, and Kate Saenko. Object hallucination in image captioning. In *Conference on Empirical Methods in Natural Language Processing*, 2018. 1, 2, 6
- [36] Rohan Taori, Ishaan Gulrajani, Tianyi Zhang, Yann Dubois, Xuechen Li, Carlos Guestrin, Percy Liang, and Tatsunori B Hashimoto. Stanford alpaca: An instruction-following llama model, 2023. 2
- [37] Hugo Touvron, Thibaut Lavril, Gautier Izacard, Xavier Martinet, Marie-Anne Lachaux, Timothée Lacroix, Baptiste Rozière, Naman Goyal, Eric Hambro, Faisal Azhar, et al. Llama: Open and efficient foundation language models. *arXiv preprint arXiv:2302.13971*, 2023.
- [38] Hugo Touvron, Louis Martin, Kevin Stone, Peter Albert, Amjad Almahairi, Yasmine Babaei, Nikolay Bashlykov, Soumya Batra, Prajjwal Bhargava, Shruti Bhosale, et al. Llama 2: Open foundation and fine-tuned chat models. *arXiv preprint arXiv:2307.09288*, 2023. 2, 5
- [39] Junyan Wang, Yi Zhou, Guohai Xu, Pengcheng Shi, Chenlin Zhao, Haiyang Xu, Qinghao Ye, Mingshi Yan, Ji Zhang, Jihua Zhu, Jitao Sang, and Haoyu Tang. Evaluation and analysis of hallucination in large vision-language models. *ArXiv*, abs/2308.15126, 2023. 2
- [40] Thomas Wolf, Lysandre Debut, Victor Sanh, Julien Chaumond, Clement Delangue, Anthony Moi, Pierric Cistac, Tim Rault, Rémi Louf, Morgan Funtowicz, Joe Davison, Sam Shleifer, Patrick von Platen, Clara Ma, Yacine Jernite, Julien Plu, Canwen Xu, Teven Le Scao, Sylvain Gugger, Mariama Drame, Quentin Lhoest, and Alexander M. Rush. Huggingface’s transformers: State-of-the-art natural language processing. *ArXiv*, abs/1910.03771, 2019. 6
- [41] Guangxuan Xiao, Yuandong Tian, Beidi Chen, Song Han, and Mike Lewis. Efficient streaming language models with attention sinks, 2024. 4
- [42] Qinghao Ye, Haiyang Xu, Jiabo Ye, Mingshi Yan, Anwen Hu, Haowei Liu, Qi Qian, Ji Zhang, Fei Huang, and Jingren Zhou. mplug-owl2: Revolutionizing multi-modal large language model with modality collaboration. *ArXiv*, abs/2311.04257, 2023. 2, 6
- [43] Qinghao Ye, Haiyang Xu, Jiabo Ye, Ming Yan, Anwen Hu, Haowei Liu, Qi Qian, Ji Zhang, and Fei Huang. mplug-owl2: Revolutionizing multi-modal large language model with modality collaboration. In *Proceedings of the IEEE/CVF Conference on Computer Vision and Pattern Recognition*, pages 13040–13051, 2024. 2
- [44] Shukang Yin, Chaoyou Fu, Sirui Zhao, Tong Xu, Hao Wang, Dianbo Sui, Yunhang Shen, Ke Li, Xingguo Sun, and Enhong Chen. Woodpecker: Hallucination correction for multimodal large language models. *ArXiv*, abs/2310.16045, 2023. 1, 2, 6, 7, 14
- [45] Tianyu Yu, Yuan Yao, Haoye Zhang, Taiwen He, Yifeng Han, Ganqu Cui, Jinyi Hu, Zhiyuan Liu, Hai-Tao Zheng, Maosong Sun, and Tat-Seng Chua. Rllm-v: Towards trustworthy mlms via behavior alignment from fine-grained correctional human feedback. *ArXiv*, abs/2312.00849, 2023. 1, 2, 3
- [46] Hang Zhang, Xin Li, and Lidong Bing. Video-llama: An instruction-tuned audio-visual language model for video understanding. *ArXiv*, abs/2306.02858, 2023. 1, 2, 12
- [47] Yuan Zhang, Chun-Kai Fan, Junpeng Ma, Wenzhao Zheng, Tao Huang, Kuan Cheng, Denis Gudovskiy, Tomoyuki Okuno, Yohei Nakata, Kurt Keutzer, et al. Sparsevlm: Visual token sparsification for efficient vision-language model inference. *arXiv preprint arXiv:2410.04417*, 2024. 2, 3, 6, 12
- [48] Zhiyuan Zhao, Bin Wang, Linke Ouyang, Xiaoyi Dong, Jiaqi Wang, and Conghui He. Beyond hallucinations: Enhancing llms through hallucination-aware direct preference optimization. *arXiv preprint arXiv:2311.16839*, 2023. 6, 12
- [49] Yiyang Zhou, Chenhang Cui, Jaehong Yoon, Linjun Zhang, Zhun Deng, Chelsea Finn, Mohit Bansal, and Huaxiu Yao. Analyzing and mitigating object hallucination in large vision-language models. *ArXiv*, abs/2310.00754, 2023. 1, 2, 3, 6

- [50] Deyao Zhu, Jun Chen, Xiaoqian Shen, Xiang Li, and Mohamed Elhoseiny. Minigpt-4: Enhancing vision-language understanding with advanced large language models. *ArXiv*, abs/2304.10592, 2023. [1](#), [2](#)
- [51] Deyao Zhu, Jun Chen, Xiaoqian Shen, Xiang Li, and Mohamed Elhoseiny. Minigpt-4: Enhancing vision-language understanding with advanced large language models. *arXiv preprint arXiv:2304.10592*, 2023. [2](#)

# VASparse: Towards Efficient Visual Hallucination Mitigation for Large Vision-Language Model via Visual-Aware Sparsification

## Supplementary Material

### 7. Experimental Details

#### 7.1. Experimental Setting

For the settings of the CHAIR and POPE benchmarks, we evaluated the results with the maximum generation token limits of LVLM  $L_{max}$  set to 64 and 512, respectively. For the GPT4-assist benchmark [48], we referred to prior work and adopted SHR Evaluation. For the GPT-4 settings, we followed the GPT4-assist configurations and used OpenAI’s gpt-4-0613 version API for evaluation. The parameters for LVLMs were set as follows: Top-k=False, Top-p=1, and Temperature=1. All our experiments, including decoding speed statistics, are conducted on Tesla A100-80G GPUs.

For the proposed token selection strategy, we do not perform sparsification at every decoding step, as this would result in excessive sparsification at each step, leading to overly short generated sequences. In practice, we perform sparsification only after decoding a certain length of new tokens, denoted as  $L_s$ . For  $L_{max} = 64$ , the beam size is set to 3, and  $L_s$  is set to 32. For  $L_{max} = 512$ , the beam size is set to 2, and  $L_s$  is set to 16. Additionally, in our method, the adaptive plausibility threshold is set to 0.1.

Regarding the comparison of VASparse with SOTAs that are specifically designed for VH mitigation, we adopt the code, hyper-parameters, and pre-trained models of each method outlined in their public repositories and papers respectively. Specifically, for DoLa [10], the parameters are set as follows: the repetition penalty is 1.2, the adaptive plausibility threshold is 0.1, and the pre-mature layers are  $[0, 2, \dots, 32]$ . For beam search-based OPERA [18] hyperparameters are set as follows: the self-attention weights scale factor is 50, the attending retrospection threshold is 15, the beam size is 3, and the penalty weights are 1. The VCD [20] hyperparameters are set as follows: the amplification factor is 1, the adaptive plausibility threshold is 0.1, and the diffusion noise step is 500. The HALC [7] hyperparameters are set as follows: the amplification factor is 0.05, the JSD buffer size is 6, the beam size is 1, the FOV sampling uses exponential expansion, the number of sampled FOVs is 4, the exponential growth factor is 0.6, and the adaptive plausibility threshold is 0.1. For post-processing methods, such as LURE and Woodpecker, we follow the settings in HALC [7]. For the SID method [19], we referred to the original configuration in their paper. For all baselines, we follow their implementations and default hyper-parameters

as reported in the paper.

#### 7.2. Setting of Empirical Studies

In Section 3, we provide our empirical observations, where all empirical studies are based on LLaVA-1.5 [46]. For the hallucination evaluation results, experiments are conducted on 500 samples randomly selected from the MSCOCO dataset. For decoding speed, we calculate the average number of tokens decoded per second by the model on the 500 samples. Token sparsification methods, such as FastV [6] and SparseVLM [47], directly prune image tokens.

### 8. Proof of Theorem 1

We aim to prove that in the following optimization problem, our strategy achieves a globally optimal solution:

$$\begin{aligned} \min_M \quad & \mathcal{E}(M) = \sum_{i=1}^L (y_i - M_i y_i)^2 - \lambda P_i M_i \\ \text{s.t.} \quad & M_i \in \{0, 1\}, \quad \forall i = 1, 2, \dots, L, \\ & \sum_{i=1}^L M_i = S, \end{aligned} \quad (9)$$

where:

- $y_i = \langle q, K_i \rangle$  is the inner product of the query vector  $q$  and the key matrix vector  $K_i$ .
- $P_i \geq 0$  is the selection probability, indicating the priority of selecting a specific element.
- $M_i \in \{0, 1\}$  denotes whether the  $i$ -th element is selected.
- The constraint requires exactly  $S$  elements in  $M$  to be 1.

The goal is to minimize the total error  $\mathcal{E}(M)$  when selecting  $S$  elements.

**Proof** First, expand and simplify the objective function  $\mathcal{E}(M)$ :

$$\begin{aligned} \mathcal{E}(M) &= \sum_{i=1}^L \left[ (y_i - M_i y_i)^2 - \lambda P_i M_i \right] \\ &= \sum_{i=1}^L \left[ y_i^2 (1 - M_i)^2 - \lambda P_i M_i \right]. \end{aligned} \quad (10)$$

Since  $M_i \in \{0, 1\}$ , it follows that  $M_i^2 = M_i$  and  $(1 - M_i)^2 = 1 - 2M_i + M_i^2 = 1 - 2M_i + M_i$ . Substituting

these simplifications, we get:

$$\begin{aligned}\mathcal{E}(M) &= \sum_{i=1}^L [y_i^2(1 - 2M_i + M_i) - \lambda P_i M_i] \\ &= \sum_{i=1}^L [y_i^2(1 - M_i) - \lambda P_i M_i].\end{aligned}\quad (11)$$

Next, remove the constant term  $\sum_{i=1}^L y_i^2$ , as it does not affect the optimization:

$$\begin{aligned}\mathcal{E}(M) &= \sum_{i=1}^L [y_i^2 - y_i^2 M_i - \lambda P_i M_i] \\ &= \sum_{i=1}^L [y_i^2 - M_i(y_i^2 + \lambda P_i)].\end{aligned}\quad (12)$$

Thus, the optimization problem can be equivalently transformed into maximizing the following objective function:

$$\begin{aligned}\max_M \quad & \sum_{i=1}^L M_i(y_i^2 + \lambda P_i) \\ \text{s.t.} \quad & M_i \in \{0, 1\}, \quad \forall i, \\ & \sum_{i=1}^L M_i = S.\end{aligned}\quad (13)$$

Our goal is now to select  $S$  elements to maximize the total reward  $\sum_{i=1}^L M_i \delta_i$ , where:

$$\delta_i = y_i^2 + \lambda P_i. \quad (14)$$

#### Characteristics of the Objective Function

- **Linearity:** The objective function is linear with respect to  $M_i$ , with no interaction terms between  $M_i$  and  $M_j$ .
- **Independence:** The contribution of each  $M_i$  to the total reward depends solely on its own  $\delta_i$ , independent of other variables  $M_j$ .

We employ the following selection strategy:

1. Compute the marginal reward  $\delta_i$  for each element:

$$\delta_i = y_i^2 + \lambda P_i. \quad (15)$$

2. Sort all elements by  $\delta_i$  in descending order.
3. Select the top  $S$  elements, setting their corresponding  $M_i$  to 1, and the rest to 0.

**Optimality of the Strategy** For any feasible solution  $M$ , we have:

$$\sum_{i=1}^L M_i = S, \quad M_i \in \{0, 1\}. \quad (16)$$

Define the total reward for a solution  $M$  as:

$$R(M) = \sum_{i=1}^L M_i \delta_i. \quad (17)$$

Let the solution chosen by our strategy be  $M^{\text{ours}}$ , with total reward:

$$R_{\text{ours}} = \sum_{i=1}^L M_i^{\text{ours}} \delta_i, \quad (18)$$

where  $M_i^{\text{ours}} = 1$  if  $i$  belongs to the top  $S$  elements with the highest  $\delta_i$ , and  $M_i^{\text{ours}} = 0$  otherwise. Since  $\delta_i$  is sorted in descending order, the elements chosen by our strategy have the highest individual scores.

For any element  $i$  in  $M$  such that  $M_i = 1$ , if its score  $\delta_i$  is smaller than that of an unselected element  $j$  (i.e.,  $M_j = 0$ ), swapping these two elements would result in a new total reward:

$$R'(M) = R(M) - \delta_i + \delta_j. \quad (19)$$

Since  $\delta_j > \delta_i$ , this increases the total reward. Thus, any feasible solution  $M$  with lower-scoring elements can always be improved by following our selection strategy.

Finally, for any feasible solution  $M$ , we have:

$$R_{\text{ours}} = \sum_{i=1}^L M_i^{\text{ours}} \delta_i \geq \sum_{i=1}^L M_i \delta_i = R(M). \quad (20)$$

**Conclusion** The total reward achieved by our algorithm is no less than that of any other feasible solution. Therefore, the solution provided by our strategy is globally optimal.

## 9. More evidence of empirical observations

We present additional evidence on the attention sparsity and attention sinking of LLaVA-1.5 in Figure 6. Our research findings confirm that the self-attention in most layers of the LVLm decoder is sparse. Furthermore, we observe a significant attention "sinking" effect on certain text tokens within the LVLm's attention mechanisms. These results further confirm the characteristics of attention sparsity and attention sinking in LVLms.

## 10. More results on CHAIR benchmark

We set the maximum generation length to 512 and evaluated our method using the CHAIR benchmark, as shown in Table 6. We can observe that when setting the maximum generation length to 512, our method still outperforms the baseline method in most metrics, while achieving competitive decoding speed. For all results, we set different random seeds and run them five times, and record the average of the results from the five runs.

## 11. More results on POPE benchmark

Following HALC [7], we utilize offline POPE (OPOPE) benchmark with both accuracy and F1-score as evaluation metrics to assess VH. We conduct experiments under two different maximum text length settings: 64 and 512 tokens. As

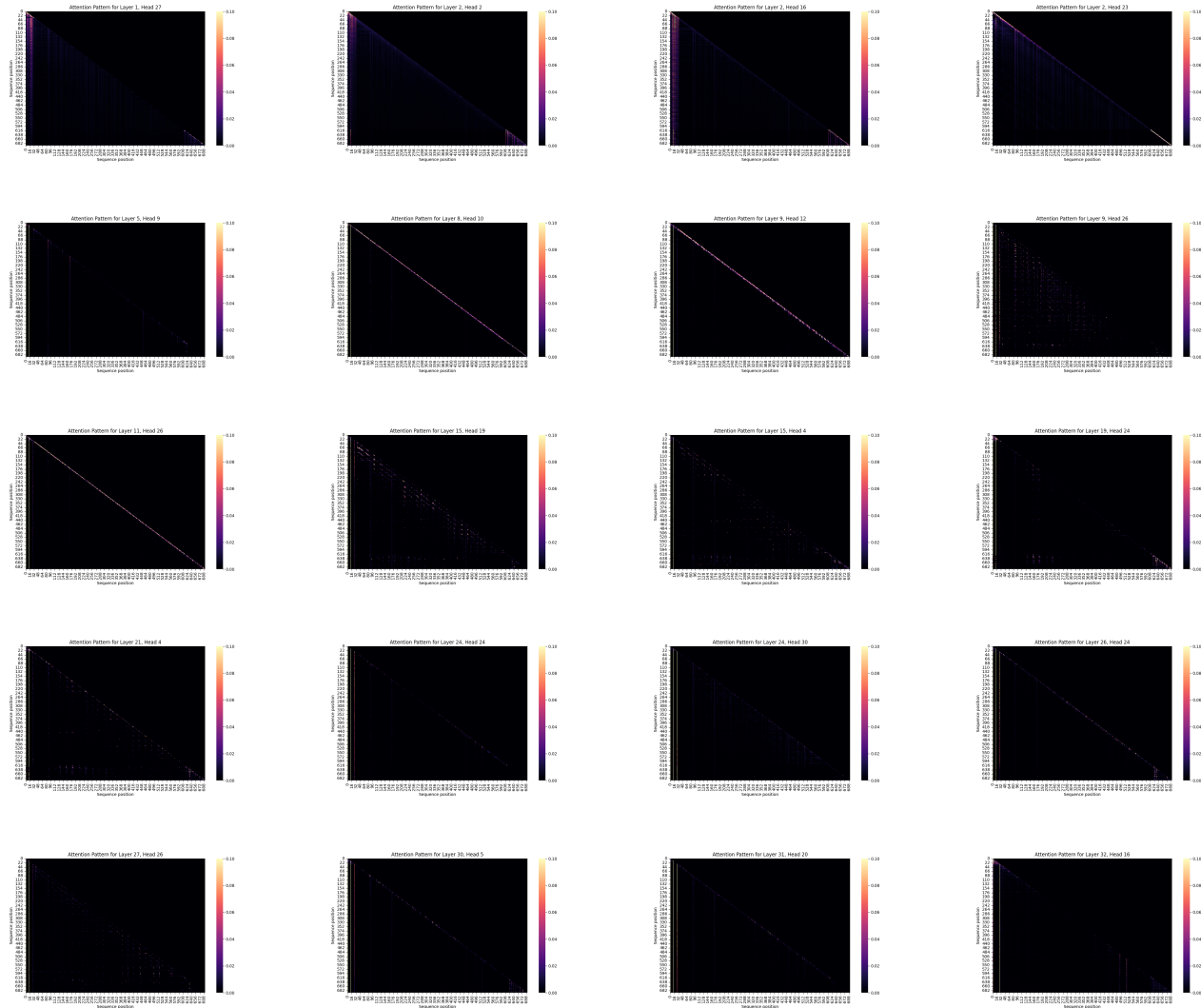


Figure 6. More visualization and evidence of sparsity of attention and sinking attention on the LLaVA-1.5.

shown in Tables 7 and 8, we observe several key findings: (1) VASparse consistently achieves optimal performance across most experimental settings, surpassing both state-of-the-art decoding methods and post-processing approaches under both the 64 and 512-token settings. (2) The effectiveness of VASparse remains robust across different text length configurations. The performance improvements persist when extending the maximum text length from 64 to 512 tokens, indicating the method’s scalability; (3) VASparse demonstrates consistent VH mitigation capabilities across three distinct LVLM architectures, highlighting its versatility and plug-and-play nature. This architectural agnosticism suggests broad applicability across different model frameworks.

## 12. Qualitative Study

To visually demonstrate the effectiveness of our approach, we present generated captions from our method and baseline approaches in Figures 7 and 8 on the MSCOCO dataset. We consistently used *Please describe this image in detail.* as the input prompt across all experiments. The results indicate that captions generated by our VASparse method exhibit notably fewer hallucinated descriptions. To further evaluate our method’s effectiveness in mitigating VH, we conducted experiments on LLaVA-Bench [27], which consists of 24 distinct images with expert-annotated descriptions and corresponding evaluation questions. In alignment with previous studies [7, 20, 44], we employed this benchmark for qualitative assessment of VH reduction. The visual results are presented in Figure 9, 10 and 11, where we consistently

Methods	LLaVA-1.5			MiniGPT-4			mPLUG-Owl2		
	CHAIR <sub>i</sub> ↓	CHAIR <sub>s</sub> ↓	TPS↑	CHAIR <sub>i</sub> ↓	CHAIR <sub>s</sub> ↓	TPS↑	CHAIR <sub>i</sub> ↓	CHAIR <sub>s</sub> ↓	TPS↑
FastV*	17.62	51.94	33.18	19.67	54.59	38.05	22.65	67.68	24.37
SparseVLM*	18.09	52.40	32.06	19.85	55.27	37.49	23.04	68.42	23.19
Woodpecker†	13.27	49.72	-	13.76	44.07	-	18.39	59.58	-
LURE†	13.08	47.95	-	13.49	43.92	-	17.85	57.73	-
Greedy	14.63	49.66	31.17	14.06	43.65	36.28	19.07	61.28	19.96
Beam Search	13.62	48.89	29.89	13.90	44.45	32.10	17.12	54.66	19.58
OPERA	12.98	47.60	4.07	15.42	42.42	5.27	17.86	56.29	3.49
VCD	14.82	49.76	17.55	17.09	43.80	17.68	19.46	62.44	9.77
DoLa	13.75	50.03	23.40	13.85	44.20	24.75	18.43	60.18	14.23
SID	13.29	47.09	19.57	13.68	43.65	22.67	18.47	60.82	12.85
HALC	12.93	46.35	2.04	13.73	43.68	3.68	17.63	56.12	1.50
Ours	<b>12.46</b>	<b>46.21</b>	27.53	<b>13.29</b>	<b>43.02</b>	29.74	<b>17.02</b>	<b>53.70</b>	17.86

Table 6. Comparison of the average CHAIR evaluation results (instance levels CHAIR<sub>i</sub> and sentence levels CHAIR<sub>s</sub>) and token per second (TPS) during decoding with different baselines on MSCOCO datasets of five random runs. \* represents the image token sparsity method and † is the post-hoc methods.

	Methods	Max New Token 512					
		Random		Popular		Adversarial	
		Accuracy	F1 score	Accuracy	F1 score	Accuracy	F1 score
LLaVA-1.5	Greedy	77.19	71.74	72.74	67.99	71.18	66.76
	Beam Search	78.38	<b>73.60</b>	75.06	70.74	72.87	<b>68.96</b>
	OPERA	78.01	72.98	74.31	69.81	73.25	68.95
	VCD	77.82	72.98	74.56	70.19	72.62	68.63
	DoLa	76.69	71.07	72.12	67.26	70.80	66.23
	SID	77.93	72.84	74.89	69.34	72.77	68.30
	HALC	77.08	72.16	74.15	69.09	72.46	68.04
	Ours	<b>78.57</b>	72.33	<b>75.16</b>	<b>70.51</b>	<b>73.37</b>	68.88
MiniGPT4	Greedy	69.14	56.55	65.84	54.04	65.67	53.91
	Beam Search	68.90	55.78	65.67	53.32	65.61	53.28
	OPERA	69.77	57.24	<b>66.90</b>	55.04	65.38	53.85
	VCD	69.32	57.05	65.14	53.89	65.25	53.98
	DoLa	69.02	56.31	66.08	54.07	65.84	53.90
	SID	69.05	56.53	65.58	53.53	65.45	53.52
	HALC	69.13	56.86	65.62	53.63	65.73	53.69
	Ours	<b>69.84</b>	<b>57.36</b>	66.31	<b>55.68</b>	<b>66.02</b>	<b>54.10</b>
mPLUG-Owl2	Greedy	76.21	70.16	71.61	81.48	69.38	64.63
	Beam Search	75.83	69.87	71.83	81.75	69.02	64.29
	OPERA	73.56	65.33	70.32	<b>84.43</b>	67.90	60.82
	VCD	75.74	69.16	70.67	80.63	69.08	63.77
	DoLa	76.33	70.22	71.67	81.72	69.55	64.71
	SID	75.72	69.31	71.79	81.90	69.12	64.10
	HALC	75.62	69.04	70.24	82.40	68.35	63.51
	Ours	<b>76.51</b>	<b>70.45</b>	<b>72.19</b>	82.44	<b>69.72</b>	<b>64.98</b>

Table 7. Comparison of the average Accuracy and F1-score evaluation results under different settings (i.e., *Random*, *Popular*, *Adversarial*) with different baselines and our VASparse on offline POPE benchmark [7, 24] of five random runs. Higher F1-score indicate better performance and bold indicates the best results. We set the maximum generated length to 512.

	Methods	Max New Token 64					
		Random		Popular		Adversarial	
		Accuracy	F1 score	Accuracy	F1 score	Accuracy	F1 score
LLaVA-1.5	Woodpecker†	70.82	59.73	68.62	58.53	68.49	58.07
	LURE†	71.10	60.08	69.17	58.63	69.16	58.34
	Greedy	70.55	58.75	68.93	57.42	67.91	56.64
	Beam Search	71.32	60.38	69.31	58.98	69.02	58.43
	OPERA	71.02	59.80	69.31	58.42	68.79	58.00
	VCD	71.08	60.05	68.96	58.34	68.55	58.02
	DoLa	70.73	59.36	69.14	58.08	68.32	57.44
	SID	71.47	61.63	69.42	59.62	69.36	58.83
	HALC	70.76	60.46	69.17	59.33	69.25	58.50
	Ours	<b>72.03</b>	<b>62.13</b>	<b>70.18</b>	<b>60.93</b>	<b>70.31</b>	<b>59.20</b>
MiniGPT4	Woodpecker†	68.05	53.84	65.49	51.70	65.06	51.27
	LURE†	68.12	53.91	65.96	52.37	65.17	51.38
	Greedy	68.02	53.71	65.31	51.68	65.41	51.92
	Beam Search	68.26	53.97	66.02	52.27	65.55	51.93
	OPERA	67.73	53.08	65.37	51.32	65.19	51.20
	VCD	67.96	53.26	65.61	51.50	65.02	51.07
	DoLa	68.08	53.83	65.55	51.93	65.25	51.72
	SID	68.09	53.86	65.69	51.98	65.28	51.77
	HALC	68.18	53.93	65.83	52.06	65.31	51.80
	Ours	<b>68.55</b>	<b>54.87</b>	<b>66.23</b>	<b>52.93</b>	<b>65.91</b>	<b>52.70</b>
mPLUG-Owl2	Woodpecker†	68.61	58.10	67.28	53.07	66.58	55.42
	LURE†	68.78	58.28	67.35	53.15	66.89	55.65
	Greedy	69.67	57.40	68.02	53.43	67.14	55.43
	Beam Search	68.79	55.31	66.92	52.89	65.90	53.12
	OPERA	69.08	55.70	67.37	53.41	66.43	53.66
	VCD	<b>70.49</b>	<b>58.63</b>	68.55	54.87	67.31	56.13
	DoLa	69.61	57.21	67.90	53.38	67.08	55.24
	SID	69.34	55.82	67.80	53.46	67.01	56.07
	HALC	69.66	56.29	67.67	53.38	66.95	55.84
	Ours	70.38	58.27	<b>68.70</b>	<b>55.28</b>	<b>67.86</b>	<b>56.77</b>

Table 8. Comparison of the average Accuracy and F1-score evaluation results under different settings (i.e., *Random*, *Popular*, *Adversarial*) with different baselines and our VASparse on offline POPE benchmark [7, 24] of five random runs. Higher F1-score indicate better performance and bold indicates the best results. † denotes the post-hoc method. We set the maximum generated length to 64.

used the prompt *Please describe this image in detail.* to generate image captions.





**VASparse (Ours):** The image features two zebras standing in a grassy field, with one of them jumping in the air. The zebra in the air appears to be performing a trick, while the other zebra stands nearby, possibly observing the action. There are several people in the scene, some of whom are watching the zebras from behind a fence. The spectators are scattered around the field, with some standing closer to the zebras and others further away.

**Greedy:** The image features a zebra and a horse standing in a grassy field, both appearing to be enjoying their time together. The zebra is positioned on the left side of the field, while the horse is on the right. There are several people in the scene, with some standing near the fence and others scattered around the field. A few individuals are closer to the zebra, while others are near the horse. **A car can be seen in the background, parked on the left side of the field.**

**HALC:** The image features a zebra and a horse in a fenced-in area, likely at a zoo or a similar facility. The zebra is in the middle of a jump, while the horse stands nearby, watching the zebra's actions. In addition to the main zebra and horse, there are a few other people scattered around the scene, some closer to the fence and others further away. **A car can be seen in the background, likely belonging to one of the visitors.**

**VCD:** In this image, there is a zebra standing on a sandy area, possibly in a zoo enclosure. The zebra appears to be in motion, possibly running or galloping. Additionally, there is a horse present in the scene, standing on the other side of a fence. There are several individuals in various positions around the fence, watching the zebra and the horse. **A car can be seen in the background, stopping by the roadside.**

**DoLa:** The image features two zebras in a grassy field, with one of them jumping in the air. The zebra in the air is positioned towards the left side of the field, while the other zebra is standing on the right side. There are several people watching the zebras from behind a wooden fence. Some of them are standing closer to the zebras, while others are positioned further away. The onlookers appear to be enjoying the sight of the zebras in action. **There are several cars parked by the fence in the distance.**

Figure 7. Qualitative results comparing our VASparse and other methods with LLaVA-1.5 backbone.



**VASparse (Ours):** The image features a blue and yellow passenger train traveling down the tracks. The train is quite long, occupying a significant portion of the scene. The train is moving along the tracks, which are surrounded by trees and bushes, creating a serene and natural environment. There are multiple train tracks visible in the image, with the main train traveling on one of them. Additionally, there are two smaller trains in the scene.

**Greedy:** The image depicts a blue and yellow train traveling down the tracks, surrounded by trees and bushes. There are multiple train tracks visible in the scene, with the main train occupying one of them. **In addition to the train, there are several traffic lights scattered throughout the image**, likely indicating the presence of intersections or crossings. **These traffic lights** are positioned at various heights and distances from the train.

**SID:** The image features a blue and yellow train traveling down the tracks, surrounded by trees. The train is moving along the tracks, and there are several other tracks visible in the scene. The train appears to be a passenger train, **as it is designed for transporting people rather than cargo**. The train's colorful design and the presence of multiple tracks suggest that this is a busy transportation hub or a well-connected railway network.

**VCD:** The image features a blue and yellow passenger train traveling down the tracks. The train is quite long, stretching across the entire width of the scene. It appears to be moving at a moderate speed, as it is not too close to the viewer. There are several traffic lights along the train tracks, with some located closer to the train and others further away. **These traffic lights are likely used to control the train's movement and ensure safe passage through the area.**

**OPERA:** The image features a blue and yellow train traveling along the railroad tracks. **It appears to be a commuter train with multiple cars**, as it passes through the countryside. There are several trees visible in the background, providing a scenic atmosphere for the train journey. The train is situated between two sets of train tracks, which indicates a well-organized transportation system.

Figure 8. Qualitative results comparing our VASparse and other methods with LLaVA-1.5 backbone.



**VASparse (Ours):** The image showcases a group of three coffee cups on a counter, each featuring a large, colorful mug with a Super Mario Bros. design. The cups are stacked in a row, with one placed in the middle and the other two on either side, creating a visually appealing display. The coffee cups are all positioned side by side, making it easy for viewers to appreciate the design and details of each cup.

**Greedy:** The image features a collection of four coffee mugs, each with a unique design. The mugs are arranged in a row, with one mug on the left, another in the middle, and two more on the right side. The mugs are all white and have a Mario theme, with each mug featuring a different Mario character. The characters are displayed in various positions, adding visual interest to the arrangement.

**OPERA:** The image showcases a collection of four coffee mugs, which featuring a different Mario character. All mugs are placed side by side, showcasing their unique designs. The Mario characters are displayed on the front of each mug, making them an appealing choice for fans of the iconic video game character.

**VCD:** The image showcases a collection of four coffee mugs, each featuring a different Mario character. The mugs are placed side by side, showcasing their unique designs. The Mario characters are prominently displayed on the front of each mug, making them an appealing choice for fans of the iconic video game character.

**SID:** The image showcases a collection of four coffee mugs, each featuring a different Mario character. The mugs are arranged in a row, with each character occupying a separate mug. The first mug on the left features a close-up of Mario's face, while the second mug on the right displays a full-body image of the iconic character. The third mug in the middle showcases a side view of Mario, and the fourth mug on the far right showcases a back view of the character.

Figure 9. LLaVA-Bench results comparing our VASparse and other methods with LLaVA-1.5 backbone.



**VASparse (Ours):** The image features a group of three animals sitting around a dining table, enjoying a meal together. The animals include a large brown bear, a cat, and a rabbit. They are all seated on the grass, with the bear on the left side, the cat in the middle, and the rabbit on the right side of the table. A plate of food is placed on the table, and there are several donuts scattered around the table. The animals are eating and drinking from cups.

**Greedy:** The image features a group of three animals sitting around a dining table, enjoying a meal together. The animals include a large brown bear, a cat, and a rabbit. They are all seated on the grass, with the bear on the left side, the cat in the middle, and the rabbit on the right side of the table. The table is set with various food items, including a cake, a bowl, and a cup. The cake is placed in the center of the table, while the bowl and cup are positioned closer to the right side.

**OPERA:** The image depicts a whimsical scene of three animals sitting around a dining table, enjoying a meal together. The table is filled with a variety of food items, including donuts, cakes, and sandwiches. The animals are positioned around the table, with a bear on the left side, a cat in the middle, and a rabbit on the right side. Each animal has a cup and a spoon placed in front of them, indicating that they are eating from bowls.

**VCD:** The image portrays a charming scene of three animals sitting at a wooden dining table. A black bear is on one side, a white cat on another side, and a rabbit on the opposite side. All three animals are eating food, with a cup placed in front of each animal. There is a plate of food on the table, and several carrots are spread out around the table. The animals appear to be enjoying their meal together, creating a whimsical and heartwarming atmosphere.

**DoLa:** The image depicts a whimsical scene of a bear, a cat, and a rabbit sitting around a dining table, enjoying a meal together. The bear is on the left side of the table, the cat is in the middle, and the rabbit is on the right side. The table is set with a variety of food items, including a cake, a bowl, and a cup. The cake is placed in the center of the table, while the bowl and cup are positioned closer to the right side. The animals seem to be enjoying their time together.

Figure 10. LLaVA-Bench results comparing our VASparse and other methods with LLaVA-1.5 backbone.



**VASparse (Ours):** The image features a close-up view of a delicious meal consisting of several cooked lobster tails. The lobster tails are accompanied by a few lemon wedges, which add a refreshing touch to the dish. The combination of the cooked lobster tails and the lemon wedges creates an appetizing and visually appealing presentation.

**Greedy:** The image showcases a close-up view of several cooked lobster tails with lemon wedges placed on top of them. The lobster tails are arranged in a visually appealing manner, with some tails overlapping each other. The lemon wedges are spread across the tails, adding a burst of citrus flavor to the dish. The combination of the cooked lobster tails and the lemon wedges creates a mouth-watering and appetizing presentation.

**HALC:** The image showcases a close-up view of several cooked lobster tails on a dining table. The lobster tails are arranged in a visually appealing manner, with some tails overlapping each other. There are a total of five lobster tails in the scene, each with varying sizes and positions. In addition to the lobster tails, there are three lemon wedges placed around the tails, adding a touch of citrus flavor to the dish. The combination of the cooked lobster tails.

**VCD:** The image features a close-up view of a delicious meal consisting of several cooked lobster tails. The tails are placed on a dining table, and they are generously seasoned with herbs and spices. The lobster tails are arranged in a visually appealing manner, with some tails overlapping each other. In addition to the lobster tails, there are a couple of lemon wedges placed on the table, adding a touch of citrus flavor to the dish.

**DoLa:** The image showcases a delectable arrangement of cooked lobster tails and lemon wedges on a dining table. There are six large lobster tails laid out, some placed next to each other, and others arranged in a visually appealing manner. The lemon wedges are scattered around the lobster tails, with a total of seven lemon wedges visible in the scene.

Figure 11. LLaVA-Bench results comparing our VASparse and other methods with LLaVA-1.5 backbone.